PHYSICAL REVIEW D **82,** 093018 (2010)

Semi-inclusive bottom-Higgs production at LHC: The complete one-loop electroweak effect in the MSSM

M. Beccaria,[1,2] G. O. Dovier,[3,4] G. Macorini,[1,2] E. Mirabella,[5] L. Panizzi,[6] F. M. Renard,[7] and C. Verzegnassi[3,4]

[1]*Dipartimento di Fisica, Università del Salento, Italy*
[2]*INFN, Sezione di Lecce, Italy*
[3]*Dipartimento di Fisica, Università di Trieste, Italy*
[4]*INFN, Sezione di Trieste, Italy*
[5]*Institut de Physique Théorique, CEA-Saclay, France*
[6]*Institut de Physique Nucléaire, Université Lyon 1 and CNRS/IN2P3, France*
[7]*Laboratoire de Physique Théorique et Astroparticules, Université Montpellier II, France*

(Received 14 May 2010; published 29 November 2010)

We present the first complete calculation of the one-loop electroweak effect in the process of semi-inclusive bottom-Higgs production at LHC in the minimal supersymmetric standard model. The size of the electroweak contribution depends on the choice of the final produced neutral Higgs boson and can be relevant, in some range of the input parameters. A comparison of the one-loop results obtained in two different renormalization schemes is also performed, showing a very good next-to-leading order scheme independence. We further comment on two possible, simpler, approximations of the full next-to-leading order result, and on their reliability.

DOI: 10.1103/PhysRevD.82.093018 PACS numbers: 12.15.Lk

I. INTRODUCTION

It is a well-known fact that $\tan\beta$ enhanced Yukawa coupling in the minimal supersymmetric standard model (MSSM) could favor the Higgs production in association with bottom quarks, contrarily to the standard model (SM) case, where the Higgs production is dominated by top-Higgs coupling.

Because of its relevance as a possible channel for the Higgs discovery, in the last few years the associated bottom-Higgs production has been extensively studied in the literature. Depending on the choice of the flavor scheme in the partonic description of the initial state and on the identified final state, one can consider a number of different partonic subprocesses for $\mathcal{H}^0 + b_{\text{jets}}$ production: while the choice of the four- versus five-flavor scheme is mainly theoretically motivated, resulting in a reordering of the perturbative expansion [1], the requirement of a minimum number of tagged b in the final state is physically relevant in the signal extraction. Assuming the five-flavor scheme (which ensures a better convergence of the perturbative series resumming large logarithms in the bottom parton distribution function (PDF), one can consider three different types of production processes, depending on the required final states: the exclusive one where both bottom jets are tagged ($b\bar{b}\mathcal{H}^0$ final state), the semi-inclusive one where only one bottom quark is tagged ($b\mathcal{H}^0$), and the inclusive one where no bottom quark jets are tagged. While the inclusive process has a larger cross section [2], the semi-inclusive with a high $p_{b,T}$ bottom in the final state is experimentally more appealing [3].

The relative weights of the partonic processes ($b\bar{b} \to \mathcal{H}^0$, $bg \to b\mathcal{H}^0$, $gg \to b\bar{b}\mathcal{H}^0$) are analyzed in [2], where also the α_s corrections (next-to-leading order [NLO]) to the leading subprocess $b\bar{b} \to \mathcal{H}^0$ are computed. The NNLO order in QCD (α_s^2) for the same subprocess is calculated in [4], while the electroweak (SM and MSSM) and SUSY-QCD NLO corrections have been computed in [5], showing that the size of electroweak corrections can be comparable, for large $\tan\beta$, with that of the strong ones.

The associated semi-inclusive production process ($b\mathcal{H}^0$ final state) is analyzed at the NLO in QCD in [3,6], while the effect of the SUSY QCD is given in [7]. Very recently, Dawson and Jaiswal have also computed, for the standard model process $bg \to bh_{\text{SM}}$, the one-loop weak corrections [8].

Finally, the exclusive process, where two bottom jets are tagged in the final state, is considered at the NLO in QCD in [1,9–11]. The leading Yukawa corrections for this partonic process are considered in [12] and SUSY-QCD effects have also been computed in [13].

Our paper is strongly motivated by the possible relevance of the associated bottom-Higgs production in the experimental search of the Higgs at the LHC; moreover, as stressed in [5], the SUSY one-loop electroweak (EW) effects (for the inclusive process) can be sizable and they can be safely accounted by an improved Born approximation. Therefore the spirit of our computation is twofold: on the one hand we provide for the first time the complete NLO EW corrections for the semi-inclusive process, including also the overall QED effect, that was not computed by [8], and on the other hand we can perform a further and independent test on the validity and limits of the improved Born approximation in different scenarios. Our calculations have been performed in two different ($\overline{\text{DR}}$ and DCPR) renormalization schemes: as expected the final one-loop results are, within at most a relative few percent difference, the same in the two frames; however, the $\overline{\text{DR}}$

scheme appears to be the one where the perturbative effect is numerically mostly more under control. Therefore we shall discuss our results in this frame, showing in various figures the dependence of the different observables on the choice of the input parameters. We have finally compared the results obtained with the full electroweak computation with those obtained within a commonly used approximation scheme. This will be done in the final part of our paper, which is organized as follows: Sec. II contains a general concentrated discussion of the actual derivation of the theoretical formulas (a part of which has been shifted in a technical Appendix B) to be used for the calculation of the various observables. Sections III and IV contain our numerical results, that are briefly discussed in Sec. V.

II. KINEMATICS AND AMPLITUDE OF THE PROCESS $bg \to b\mathcal{H}^0$

A. Kinematics

At lowest order there is only one partonic[1] channel leading to bottom-Higgs production

$$b(p_b)g(p_g) \to b(p_b')\mathcal{H}^0(p_{\mathcal{H}^0}), \tag{1}$$

where $\mathcal{H}^0$ is one of the three MSSM neutral Higgs bosons (h^0, H^0, A^0). In the partonic center-of-mass frame the momenta of the particles read

$$\begin{aligned} p_b &= (E_b; 0, 0, p), \\ p_g &= (p; 0, 0, -p), \\ p_b' &= (E_b'; p'\sin\theta, 0, p'\cos\theta), \\ p_{\mathcal{H}^0} &= (E_{\mathcal{H}^0}; -p'\sin\theta, 0, -p'\cos\theta). \end{aligned} \tag{2}$$

The Mandelstam variables are defined as

$$s = (p_g + p_b)^2, \qquad t = (p_b - p_b')^2, \qquad u = (p_g - p_b')^2. \tag{3}$$

For later convenience we define two momenta q and q' as follows:

$$q = p_b + p_g, \qquad q' = p_b' - p_g.$$

B. Born and one-loop amplitudes

We denote the $\mathcal{O}(\alpha_s^a \alpha^b)$ contribution to the amplitude (differential cross section) of the process X as $\mathcal{M}_X^{a,b}$ $(d\sigma_X^{ab})$. The Born terms result from the s- and u-channel

[1]One should also consider the photon induced process $b\gamma \to b\mathcal{H}^0$: the contribution to the total cross section arising from this subprocess is doubly suppressed, due to the smaller γ parton distribution function and smaller coupling (α instead of α_s). Because the main goal of this paper is the calculation of the NLO electroweak effects for $b\mathcal{H}^0$ production, and the $b\gamma \to b\mathcal{H}^0$ can be safely computed at the LO, we do not take into account the photon induced production in the following.

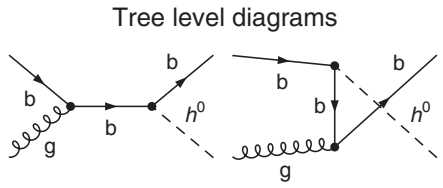

FIG. 1. Tree-level diagrams for the partonic $bg \to b\mathcal{H}^0$ processes.

b quark exchange of Fig. 1. The color stripped tree-level amplitude reads as follows:

$$\begin{aligned} \mathcal{M}_{bg\to b\mathcal{H}^0}^{1/2,1/2} = &-\left(\frac{g_s}{s - m_b^2}\right)\bar{u}_b'(\lambda_b')[c^L(bb\mathcal{H}^0)P_L \\ &+ c^R(bb\mathcal{H}^0)P_R](\not{q} + m_b)\not{\epsilon}_g(\mu)u_b(\lambda_b) \\ &- \left(\frac{g_s}{u - m_b^2}\right)\bar{u}_b'(\lambda_b')\not{\epsilon}_g(\mu)(\not{q}' + m_b) \\ &\times [c^L(bb\mathcal{H}^0)P_L + c^R(bb\mathcal{H}^0)P_R]u_b(\lambda_b), \end{aligned} \tag{4}$$

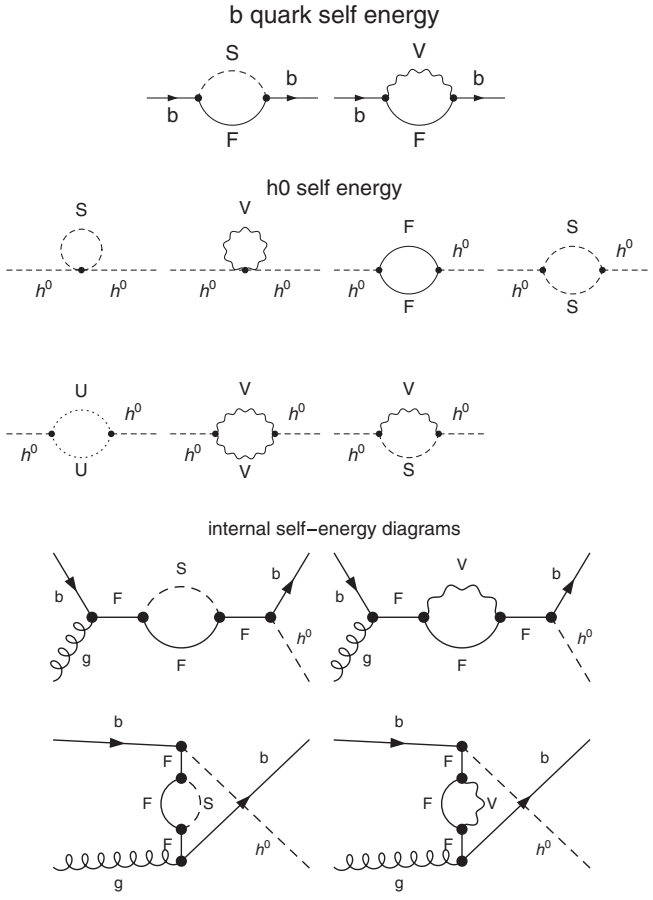

FIG. 2. Bottom quark self-energies, Higgs self-energies (only the diagonal case), and internal self-energies.

where λ_b (λ_b') is the helicity of the initial (final) bottom quark while μ is the polarization of the gluon. $u_b(\lambda_b)$ [$u_b'(\lambda_b')$] is the spinor of the initial [final] bottom quark, $\epsilon_g(\mu) = (0; \mu/\sqrt{2}, -i/\sqrt{2}, 0)$ is the gluon polarization vector, and $P_{R,L} = (1 \pm \gamma^5)/2$ are the chirality projectors. The relevant couplings $c^\eta(bb\mathcal{H}^0)$ ($\eta = L, R$) are defined as

$$
\begin{aligned}
c^\eta(bbH^0) &= -\left(\frac{em_b}{2s_W M_W}\right)\frac{\cos\alpha}{\cos\beta}, \\
c^\eta(bbh^0) &= \left(\frac{em_b}{2s_W M_W}\right)\frac{\sin\alpha}{\cos\beta} \\
c^L(bbA^0) &= -i\left(\frac{em_b}{2s_W M_W}\right)\tan\beta, \\
c^R(bbA^0) &= c^{L*}(bbA^0).
\end{aligned}
\tag{5}
$$

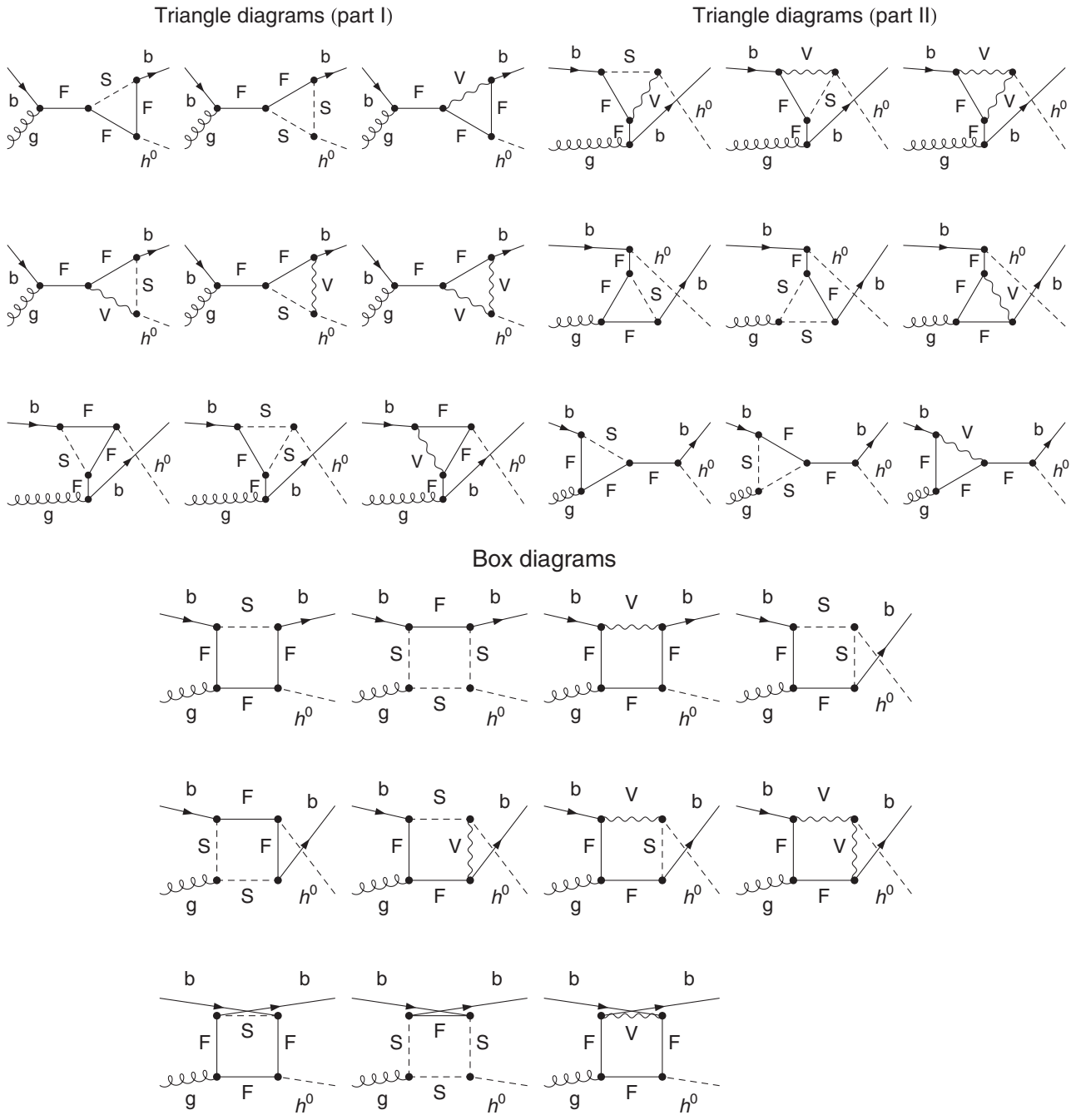

FIG. 3. Triangle and box diagrams.

We factorize out of the gluon couplings the color matrix element $\lambda^a/2$. The sum over colors leads to a factor

$$\sum_{a=1}^{8} \mathrm{tr}\left\{\frac{\lambda^a}{2}\frac{\lambda^a}{2}\right\} = 4 \tag{6}$$

that multiplies the squared amplitude.

The generic helicity amplitude can be decomposed on a set of eight forms factors $J^{k\eta}$ ($\eta = L, R$) as follows:

$$\mathcal{M}^{1/2,1/2}_{bg\to b\mathcal{H}^0} = \bar{u}'_b(\lambda'_b)\Big(\sum_{k=1}^{4}\sum_{\eta=L,R} J^{k\eta} N^{k\eta}_{bg\to b\mathcal{H}^0}\Big)u_b(\lambda_b), \tag{7}$$

where

$$\begin{aligned} J_{1\eta} &= \not{p}_g \not{\epsilon}_g(\mu) P_\eta, \qquad & J_{2\eta} &= (\epsilon_g(\mu).p'_b) P_\eta, \\ J_{3\eta} &= \not{\epsilon}_g(\mu) P_\eta, \qquad & J_{4\eta} &= (\epsilon_g(\mu).p'_b)\not{p}_g P_\eta. \end{aligned} \tag{8}$$

The only nonzero scalar functions at the tree level are $N^{1\eta}_{bg\to b\mathcal{H}^0}$ and $N^{2\eta}_{bg\to b\mathcal{H}^0}$. They read as follows:

$$\begin{aligned} N^{1\eta}_{bg\to b\mathcal{H}^0} &= -g_s\frac{c^\eta(bb\mathcal{H}^0)}{s-m_b^2} - g_s\frac{c^\eta(bb\mathcal{H}^0)}{u-m_b^2}, \\ N^{2\eta}_{bg\to b\mathcal{H}^0} &= -2g_s\frac{c^\eta(bb\mathcal{H}^0)}{u-m_b^2} \end{aligned} \tag{9}$$

The one-loop electroweak virtual contributions arise from self-energy, vertex, and box diagrams. Counterterms for the various bottom-quark lines, for the $\mathcal{H}^0$ line, and for the $bb\mathcal{H}^0$ coupling constants have to be considered as well. The corresponding diagrams can be read off from Figs. 2 and 3.

All these contributions have been computed using the usual decomposition in terms of Passarino-Veltman functions and the complete amplitude has been implemented in a C++ numerical code.

C. Renormalization

In order to cancel the ultraviolet (UV) divergences the Higgs sector and the bottom sector have to be renormalized at $\mathcal{O}(\alpha)$. The expressions of the counterterms entering our calculation are collected in Appendix B.

1. Higgs sector

As anticipated we performed the calculation using two different renormalization schemes: the $\overline{\mathrm{DR}}$ scheme [14] is defined by the following renormalization conditions:

$$\begin{aligned} \delta Z^{\overline{\mathrm{DR}}}_{H_1} &= -\left[\mathrm{Re}\frac{\partial\Sigma_{H^0}(k^2)}{\partial k^2}\bigg|_{k^2=M^2_{H^0},\alpha=0}\right]_{\mathrm{div}} \\ \delta Z^{\overline{\mathrm{DR}}}_{H_2} &= -\left[\mathrm{Re}\frac{\partial\Sigma_{h^0}(k^2)}{\partial k^2}\bigg|_{k^2=M^2_{h^0},\alpha=0}\right]_{\mathrm{div}} \\ \delta T_{h^0} &= -T_{h^0} \\ \delta T_{H^0} &= -T_{H^0} \\ \delta M^2_{A^0} &= \mathrm{Re}\Sigma_{A^0}(M^2_{A^0}) - M^2_{A^0}\Sigma'_{A^0}(M^2_{A^0}) \\ \delta\tan\beta^{\overline{\mathrm{DR}}} &= \frac{1}{2}(\delta Z^{\overline{\mathrm{DR}}}_{H_2} - \delta Z^{\overline{\mathrm{DR}}}_{H_1})\tan\beta. \end{aligned} \tag{10}$$

$\delta Z^{\overline{\mathrm{DR}}}_{H_i}$ define the wave-function renormalization constant of the Higgs field H_i, the third and fourth line fix the tadpole renormalization and the last one the $\tan\beta$ renormalization constant. $[\mathcal{A}]_{\mathrm{div}}$ means keeping the UV divergent part of $\mathcal{A}$, discarding the finite contribution. In the DCPR scheme [15,16] the independent parameters are the same, and the renormalization conditions of the Higgs wave functions change as follows:

$$\begin{aligned} \delta Z^{\mathrm{DCPR}}_{H_1} &= -\mathrm{Re}\frac{\partial\Sigma_{A^0}(k^2)}{\partial k^2}\bigg|_{k^2=M^2_{A^0}} - \frac{1}{\tan\beta M_Z}\mathrm{Re}\Sigma_{A^0Z}(M^2_{A^0}) \\ \delta Z^{\mathrm{DCPR}}_{H_2} &= -\mathrm{Re}\frac{\partial\Sigma_{A^0}(k^2)}{\partial k^2}\bigg|_{k^2=M^2_{A^0}} + \frac{\tan\beta}{M_Z}\mathrm{Re}\Sigma_{A^0Z}(M^2_{A^0}) \\ \delta T_{h^0} &= -T_{h^0} \\ \delta T_{H^0} &= -T_{H^0} \\ \delta M^2_{A^0} &= \mathrm{Re}\Sigma_{A^0}(M^2_{A^0}) - M^2_{A^0}\Sigma'_{A^0}(M^2_{A^0}) \\ \delta\tan\beta^{\mathrm{DCPR}} &= \frac{1}{2}(\delta Z^{\mathrm{DCPR}}_{H_2} - \delta Z^{\mathrm{DCPR}}_{H_1})\tan\beta. \end{aligned} \tag{11}$$

We choose to impose the on-shell (OS) condition for the mass of CP-odd A^0 Higgs in both schemes.

The renormalization constants of the Higgs bosons wave functions and of the $c^\eta(bb\mathcal{H}^0)$ couplings can be written in terms of the of the renormalization constants defined above. Their explicit expression is given in Appendix A.

2. Bottom sector

The mass of the bottom and its wave-function renormalization function is fixed in the on-shell scheme,

$$\begin{aligned} \delta m_b^{\mathrm{OS}} &= \frac{1}{2}m_b[\mathrm{Re}\Sigma_{b_L}(m_b^2) + \mathrm{Re}\Sigma_{b_R}(m_b^2) + 2\,\mathrm{Re}\Sigma_{b_S}(m_b^2)], \\ \delta Z_b^L &= -\mathrm{Re}\Sigma_{b_L}(m_b^2) - m_b^2\frac{\partial}{\partial k^2}\mathrm{Re}[\Sigma_{b_L}(k^2) + \Sigma_{b_R}(k^2) \\ &\quad + 2\Sigma_{b_S}(k^2)]|_{k^2=m_b^2}, \\ \delta Z_b^R &= -\mathrm{Re}\Sigma_{b_R}(m_b^2) - m_b^2\frac{\partial}{\partial k^2}\mathrm{Re}[\Sigma_{b_L}(k^2) + \Sigma_{b_R}(k^2) \\ &\quad + 2\Sigma_{b_S}(k^2)]|_{k^2=m_b^2}, \end{aligned} \tag{12}$$

where the bottom self-energies are defined according to following Lorentz decomposition:

$$\Sigma_b(p) = \not{p} P_L \Sigma_{b_L}(p^2) + \not{p} P_R \Sigma_{b_R}(p^2) + m_b \Sigma_{b_S}(p^2). \quad (13)$$

The bottom masses in the Yukawa couplings are treated completely at the electroweak level, with OS or $\overline{\text{DR}}$ renormalization conditions, respectively, in the two schemes. Resummation of large logarithms from the running of the bottom mass suggests to trade bottom mass appearing in the couplings with an effective bottom mass [17]. The resummation of the $(\alpha_s \tan\beta)^n$ contributions can be achieved modifying the tree-level relation between the bottom Yukawa coupling and the bottom mass: the bottom mass of the couplings, which is related to the bottom Yukawa coupling, is replaced by an effective mass (e.g. in the $\overline{\text{DR}}$ scheme)

$$m_b^{\overline{\text{DR}}} \to \bar{m}_b^{\overline{\text{DR}}} = \frac{m_b^{\overline{\text{DR}}}}{1 + \Delta_b}, \quad (14)$$

where Δ_b is given by

$$\Delta_b = \frac{2}{3}\frac{\alpha_s}{\pi} M_{\tilde{g}} \mu \tan\beta I(M_{\tilde{b}_1}, M_{\tilde{b}_2}, M_{\tilde{g}})$$

$$I(a,b,c) = \frac{-1}{(a^2-b^2)(b^2-c^2)(c^2-a^2)} \times \left(a^2 b^2 \ln\frac{a^2}{b^2} + b^2 c^2 \ln\frac{b^2}{c^2} + c^2 a^2 \ln\frac{c^2}{a^2}\right). \quad (15)$$

Moreover, the $b\bar{b}H_1$ coupling is dynamically generated at $\mathcal{O}(\alpha_s)$ and can be enhanced if $\tan\beta$ is large. This effect can be included modifying the $c^\eta(bb\mathcal{H}^0)$ couplings. The actual effect of this modification and of the bottom mass resummation, Eq. (14), is to substitute the $c^\eta(bb\mathcal{H}^0)$ couplings in Eq. (5) as follows:

$$c^\eta(bbh^0) \to \frac{c^\eta(bbh^0)}{m_b} \times \bar{m}^{\overline{\text{DR}}}\left(1 - \frac{\Delta_b}{\tan\beta \tan\alpha}\right)$$
$$c^\eta(bbH^0) \to \frac{c^\eta(bbH^0)}{m_b} \times \bar{m}^{\overline{\text{DR}}}\left(1 + \frac{\Delta_b \tan\alpha}{\tan\beta}\right) \quad (16)$$
$$c^\eta(bbA^0) \to \frac{c^\eta(bbA^0)}{m_b} \times \bar{m}^{\overline{\text{DR}}}\left(1 - \frac{\Delta_b}{\tan^2\beta}\right).$$

We have checked the cancellation of the UV divergences among counterterms, self-energies, and triangles. This cancellation occurs separately inside 8 sectors, i.e. s-channel "initial" triangles with chirality L or R, s-channel "final" L or R, u-channel up triangles (L or R) and u-channel down triangles (L or R). The box diagrams are UV-finite.

D. QED radiation

The infrared (IR) singularities affecting the virtual contributions are canceled including the bremsstrahlung of real photons at $\mathcal{O}(\alpha_s \alpha^2)$,

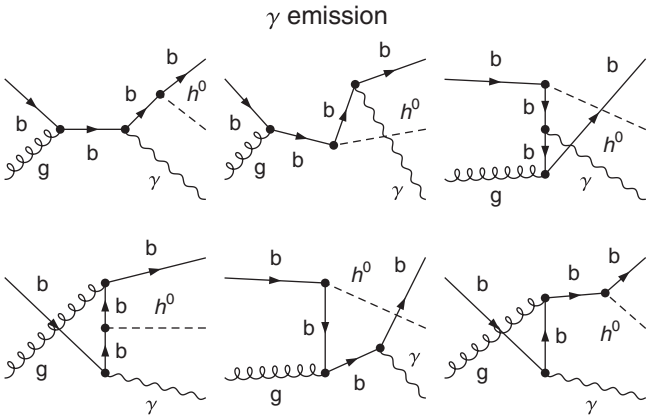

FIG. 4. Real photon γ emission.

$$b(p_b) g(p_g) \to b(p_b') \mathcal{H}^0(p_{\mathcal{H}^0}) \gamma(p_\gamma), \quad (17)$$

arising from the diagrams in Fig. 4. This contribution has been computed using FEYNARTS [18] and FORMCALC [19]. The integral over the photon phase space is IR divergent in the soft-photon region, i.e. for $p_\gamma^0 \to 0$. The IR divergences are regularized within mass regularization, giving a small

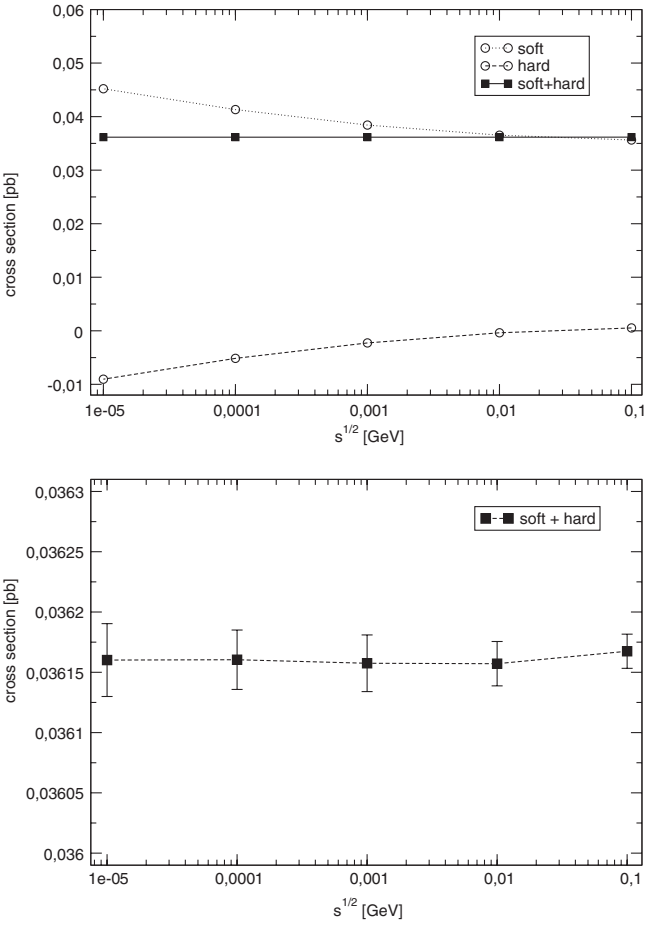

FIG. 5. A^0 production: dependence of the $\mathcal{O}(\alpha)$ soft + virtual, hard, and total sum corrections on the separator ΔE.

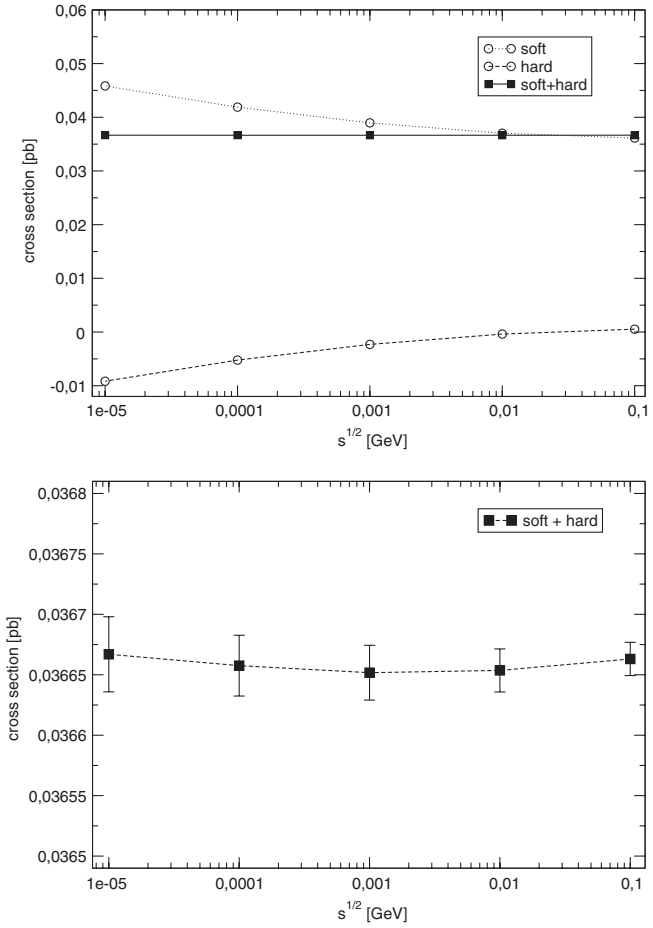

FIG. 6. H^0 production: dependence of the $\mathcal{O}(\alpha)$ soft + virtual, hard, and total sum corrections on the separator ΔE.

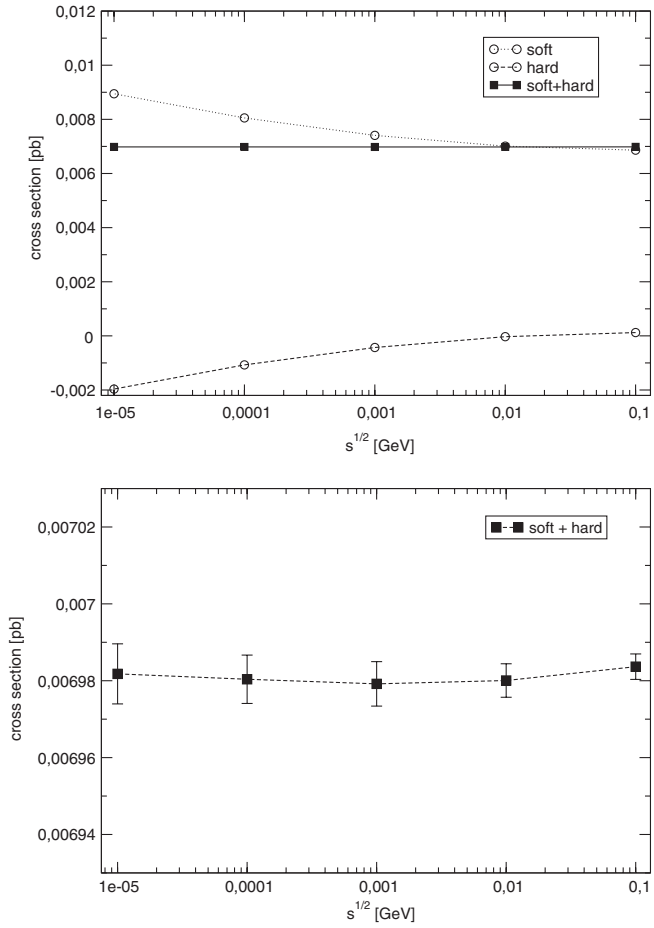

FIG. 7. h^0 production: dependence of the $\mathcal{O}(\alpha)$ soft + virtual, hard, and total sum corrections on the separator ΔE.

mass m_γ to the photon. The phase space integration has been performed using the phase space slicing method. This method introduces a fictitious separator ΔE and restricts the numerical phase space integration in the region characterized by $p_\gamma > \Delta E$. The integral over the region $p_\gamma < \Delta E$ is performed analytically in the eikonal approximation [20].

Large collinear logarithms containing the bottom mass can be reabsorbed into the redefinition of the parton distribution function of the bottom $f_b(x, \mu)$. In the $\overline{\text{MS}}$ (deep inelastic scattering [DIS]) factorization scheme this is achieved performing the substitution [21]

$$\begin{aligned} f_b(x,\mu) \to f_b(x,\mu)\Big\{1 - \frac{\alpha}{\pi} e_b^2 \Big[1 - \ln\delta_s - \ln\delta_s^2 \\ + \Big(\ln\delta_s + \frac{3}{4}\Big)\ln\Big(\frac{\mu^2}{m_b^2}\Big) - \frac{1}{4}\lambda_{\text{FC}}\kappa_1 \Big]\Big\} - \frac{\alpha}{2\pi} e_b^2 \\ \times \int_x^{1-\delta_s} \frac{dz}{z} f_b\Big(\frac{x}{z}, \mu\Big)\Big[\frac{1+z^2}{1-z}\ln\Big(\frac{\mu^2}{m_b^2}\frac{1}{(1-z)^2}\Big) \\ - \frac{1+z^2}{1-z} + \lambda_{\text{FC}}\kappa_2\Big], \end{aligned} \tag{18}$$

and setting $\lambda_{\text{FC}} = 0$ ($\lambda_{\text{FC}} = 1$). μ is the factorization scale, $\delta_s = 2\Delta E/\sqrt{s}$, while e_b is the bottom charge. κ_1 and κ_2 are defined as follows:

$$\begin{aligned} \kappa_1 &= 9 + \frac{2}{3}\pi^2 + 3\ln\delta_s - 2\ln^2\delta_s, \\ \kappa_2 &= \frac{1+z^2}{1-z}\ln\Big(\frac{1-z}{z}\Big) - \frac{3}{2}\frac{1}{1-z} + 2z + 3. \end{aligned} \tag{19}$$

We tested numerically the cancellation of IR divergences, the independence of our results of m_γ (in the sum of the soft and virtual part), and of the separator ΔE (see Figs. 5–7).

E. Total cross sections

Including the finite wave-function renormalization for the Higgs field we obtain the following expressions for the tree-level differential partonic cross section of the processes we are considering:

$$d\hat{\sigma}^{1,1}_{bg\to b\mathcal{H}^0} = \frac{\beta' d\cos\theta}{768\pi s\beta} Z_{\mathcal{H}^0} |\mathcal{M}^{1/2,1/2}_{bg\to b\mathcal{H}^0}|^2, \tag{20}$$

where $\beta = 2p/\sqrt{s}$, $\beta' = 2p'/\sqrt{s}$, and s is the Mandelstam variable defined in Eq. (3); the NLO-EW contribution to the differential cross section reads as follows:

$$
\begin{aligned}
d\hat{\sigma}^{1,2}_{bg\to bh^0} &= \frac{\beta' d\cos\theta}{768\pi s\beta} Z_{h^0}\left\{\left|1 - Z_{h^0H^0}\frac{\cos\alpha}{\sin\alpha}\right|^2 |\mathcal{M}^{1/2,1/2}_{bg\to bh^0}|^2 + 2\,\mathrm{Re}\mathcal{M}^{1/2,1/2}_{bg\to bh^0}(\mathcal{M}^{1/2,3/2}_{bg\to bh^0})^*\right\} - d\hat{\sigma}^{1,1}_{bg\to bh^0},\\
d\hat{\sigma}^{1,2}_{bg\to bH^0} &= \frac{\beta' d\cos\theta}{768\pi s\beta} Z_{H^0}\left\{\left|1 - Z_{H^0h^0}\frac{\sin\alpha}{\cos\alpha}\right|^2 |\mathcal{M}^{1/2,1/2}_{bg\to bH^0}|^2 + 2\,\mathrm{Re}\mathcal{M}^{1/2,1/2}_{bg\to bH^0}(\mathcal{M}^{1/2,3/2}_{bg\to bH^0})^*\right\} - d\hat{\sigma}^{1,1}_{bg\to bH^0},\\
d\hat{\sigma}^{1,2}_{bg\to bA^0} &= \frac{\beta' d\cos\theta}{768\pi s\beta} Z_{A^0}\{2\,\mathrm{Re}\mathcal{M}^{1/2,1/2}_{bg\to bA^0}(\mathcal{M}^{1/2,3/2}_{bg\to bA^0})^*\},
\end{aligned}
\tag{21}
$$

where the Z factors Z_{h^0}, Z_{H^0}, Z_{A^0}, $Z_{h^0H^0}$, and $Z_{H^0h^0}$ in the two renormalization schemes we are considering can be found in [14] and in [15]. The partonic differential cross section for the real photon radiation process reads as follows:

$$
d\hat{\sigma}^{1,2}_{bg\to b\mathcal{H}^0\gamma} = \frac{1}{4\cdot 24}\frac{d\phi(p'_b, p_{\mathcal{H}^0}, p_\gamma)}{2\beta s} Z_{\mathcal{H}^0}|\mathcal{M}^{1/2,1}_{bg\to b\mathcal{H}^0\gamma}|^2, \tag{22}
$$

where, according to the notation introduced in [22], $d\phi(p'_b, p_{\mathcal{H}^0}, p_\gamma)$ is the three-particles phase space measure. The hadronic differential cross section at $\mathcal{O}(\alpha_s\alpha)$ and $\mathcal{O}(\alpha_s\alpha^2)$ reads

$$
\begin{aligned}
d\sigma^{1,1}_{PP\to b\mathcal{H}^0}(S) &= \int_0^1 dx_1 \int_0^1 dx_2[f_b(x_1,\mu)f_g(x_2,\mu) + (x_1\leftrightarrow x_2)]d\hat{\sigma}^{1,1}_{bg\to b\mathcal{H}^0}(x_1x_2S)\\
d\sigma^{1,2}_{PP\to b\mathcal{H}^0(\gamma)}(S) &= \int_0^1 dx_1 \int_0^1 dx_2[f_b(x_1,\mu)f_g(x_2,\mu) + (x_1\leftrightarrow x_2)][d\hat{\sigma}^{1,2}_{bg\to b\mathcal{H}^0}(x_1x_2S) + d\hat{\sigma}^{1,2}_{bg\to b\mathcal{H}^0\gamma}(x_1x_2S)],
\end{aligned}
\tag{23}
$$

respectively. $\sqrt{S}$ is the hadronic center-of-mass energy, while $f_i(x_i,\mu)$ is the parton distribution function of the parton i inside the proton with a momentum fraction x_i at the scale μ. For later convenience we define the invariant mass distribution as

$$
\begin{aligned}
\frac{d\sigma^{1,1}_{PP\to b\mathcal{H}^0}}{d\sqrt{\hat{s}}} &= \int_0^1 dx_1 \int_0^1 dx_2[f_b(x_1,\mu)f_g(x_2,\mu) + (x_1\leftrightarrow x_2)]d\hat{\sigma}^{1,1}_{bg\to b\mathcal{H}^0}(x_1x_2S) \times \delta(\sqrt{x_1x_2S} - \sqrt{\hat{s}})\\
\frac{d\sigma^{1,2}_{PP\to b\mathcal{H}^0}}{d\sqrt{\hat{s}}} &= \int_0^1 dx_1 \int_0^1 dx_2[f_b(x_1,\mu)f_g(x_2,\mu) + (x_1\leftrightarrow x_2)][d\hat{\sigma}^{1,2}_{bg\to b\mathcal{H}^0}(x_1x_2S) + d\hat{\sigma}^{1,2}_{bg\to b\mathcal{H}^0\gamma}(x_1x_2S)]\delta(\sqrt{x_1x_2S} - \sqrt{\hat{s}}).
\end{aligned}
\tag{24}
$$

III. NUMERICAL RESULTS

The independent input parameters in the MSSM Higgs sector are the A^0 mass and $\tan\beta$: since we impose the same renormalization condition for M_{A^0} only $\tan\beta$ should be converted in the change of scheme, using the one-loop relation

$$
\tan\beta^{\mathrm{DCPR}} = \tan\beta^{\overline{\mathrm{DR}}} + \delta\tan\beta^{\overline{\mathrm{DR}}} - \delta\tan\beta^{\mathrm{DCPR}}, \tag{25}
$$

while the OS and $\overline{\mathrm{DR}}$ bottom masses m_b^{OS} and $m_b^{\overline{\mathrm{DR}}}(\mu)$ are computed starting from $m_b^{\overline{\mathrm{MS}}}(m_b) = 4.2$ GeV and following the procedure described in Sec. 3.2.2 of [17].

For the numerical evaluations we defined the supersymmetric scenario SPP_1 and a class of points of the parameter space SPP_2, with variable $\tan\beta = 10, 20, 30, 40$. The input parameters characterizing these scenarios are summarized in Table I. The sparticle masses and mixing angles have been obtained with the code FEYNHIGGS [23]. The one-loop

TABLE I. Input parameters for the SUSY scenarios considered in our numerical discussion. $M_{\tilde{q},j}$ is the common value of the breaking parameters in the sector of the squarks belonging to the jth generation. The dimensionful parameters are given in GeV.

Scenario	$\tan\beta$	M_{A^0}	$M_{\tilde{q},1}$	$M_{\tilde{q},2}$	$M_{\tilde{q},3}$	M_1	M_2	$M_{\tilde{g}}$
SPP_1	15	350	350	350	250	90	150	800
SPP_2	variable	250	500	500	400	90	200	800

Higgs masses are numerically computed by finding the zero of inverse one-loop propagator matrix determinant

$$[k^2 - M^2_{H^0} + \hat{\Sigma}_{H^0}(k^2)][k^2 - M^2_{h^0} + \hat{\Sigma}_{h^0}(k^2)] - \hat{\Sigma}^2_{H^0 h^0}(k^2) = 0. \quad (26)$$

Since we require semi-inclusive production (i.e. the bottom quark must be tagged) we impose the following kinematical cuts on the bottom in the final state, limiting the transferred momentum $p_{b,T} > 20$ GeV (due to resolution limitations of the hadronic calorimeter) and the rapidity $|y_b| < 2$ (in order to be able to perform inner tracking). The process we are considering is leading order in QCD. Therefore, analogously to [24–26], we use a LO QCD PDF set, namely, the LO CTEQ6L [27]. Our choice is justified since the QED effects in the Dokshitzer-Gribov-Lipatov-Altarelli-Parisi evolution equations are known to be small [28]. The factorization of the bottom PDF has been performed in the DIS scheme, with factorization scale $\mu = M_{\mathcal{H}^0} + m_b^{\rm OS}$.

In Figs. 8–10 we show the total cross section for A^0, H^0, and h^0 production in the class of supersymmetric scenarios $\rm SPP_2$, as functions of $\tan\beta$. We present both the results in the $\overline{\rm DR}$ and in the DCPR schemes. The numerical values and the K-factors in the two schemes (defined as usual as the ratios $\sigma^{\rm NLO}/\sigma^{\rm LO}$; note that the LO is computed with the resummed/modified SUSY-QCD coupling, so our K-factors account of the pure electroweak NLO effect), as well as the ratios of the NLO cross sections in the two scheme are reported in Table II, III, and IV.

As one sees, the values of the total cross sections do coincide in the overall range, apart from small differences of the few percent size for very large $\tan\beta$ values. This confirms our expectation that at the NLO level the two schemes should be equivalent, and also provides an important check of the reliability of our calculations.

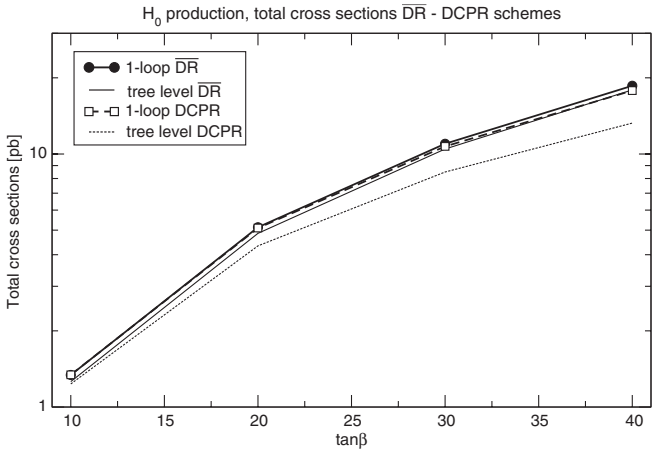

FIG. 9. Total LO and NLO cross sections in the $\overline{\rm DR}$ and DCPR schemes, H^0 production; $M_{A^0} = 250$ GeV, $p_{b,T} > 20$ GeV, $|y_b| < 2$.

Having verified the realistic one-loop equivalence of the two schemes, we have decided to perform our analysis in the $\overline{\rm DR}$ scheme. The main theoretical reasons of our choice have been fully illustrated in [29]. In particular this scheme is known to be generally more stable numerically: our results confirm mainly this expectation but it is worth noting that for h^0 production both schemes can produce (in different $\tan\beta$ regions) relatively large effects; nevertheless the good agreement between the two schemes leads one to suppose that the perturbative expansion is well behaved, and NNLO effects are well under control.

Figure 11 shows the K-factors for the three Higgs bosons in $\overline{\rm DR}$ as function of $\tan\beta$ while Figs. 12–14 show, for the scenario $\rm SPP_2$ $\tan\beta = 30$, the invariant mass distribution and the relative NLO effect. In the next Figs. 15–17 we again plot the differential distributions for the $\rm SPP_1$ scenario; the total cross sections for this scenario are reported in Table V.

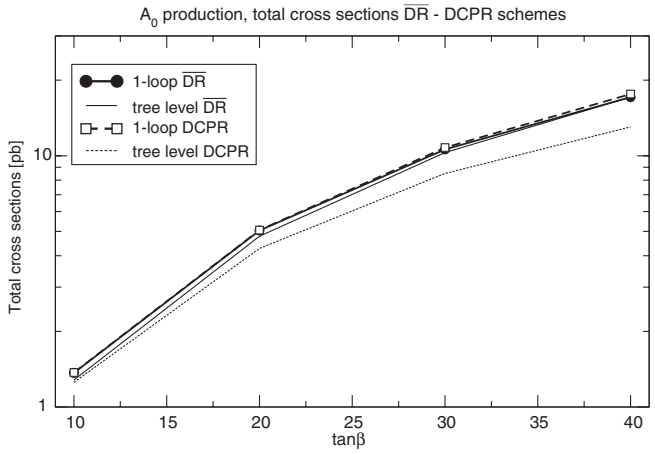

FIG. 8. Total LO and NLO cross sections in the $\overline{\rm DR}$ and DCPR schemes, A^0 production; $M_{A^0} = 250$ GeV, $p_{b,T} > 20$ GeV, $|y_b| < 2$.

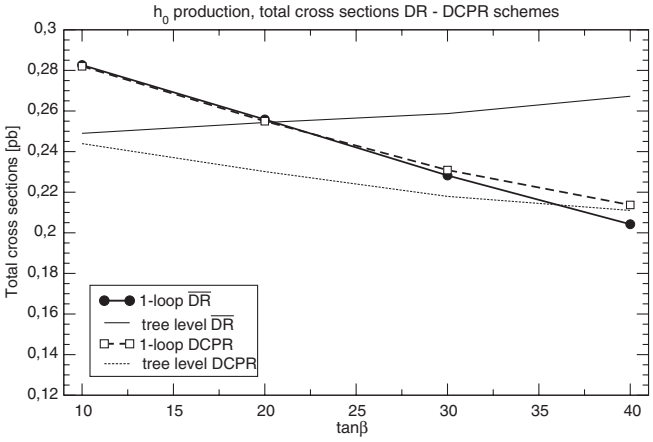

FIG. 10. Total LO and NLO cross sections in the $\overline{\rm DR}$ and DCPR schemes, h^0 production; $M_{A^0} = 250$ GeV, $p_{b,T} > 20$ GeV, $|y_b| < 2$.

TABLE II. A^0 production, SPP_2 spectra: total cross sections (pb), K-factors, and NLO $\overline{DR}$/DCPR ratio.

$\tan\beta$	$\sigma^{\overline{DR},NLO}$	$\sigma^{\overline{DR},LO}$	$\sigma^{DCPR,NLO}$	$\sigma^{DCPR,LO}$	$K^{\overline{DR}}$	K^{DCPR}	NLO ratio
10	1.367	1.281	1.371	1.253	1.067	1.093	0.997
20	5.040	4.784	5.060	4.278	1.053	1.182	0.995
30	10.601	10.295	10.785	8.505	1.029	1.268	0.98
40	17.118	17.125	17.615	13.038	0.999	1.350	0.97

TABLE III. H^0 production SPP_2 spectra: total cross sections (pb), K-factors and NLO $\overline{DR}$/DCPR ratio.

$\tan\beta$	$\sigma^{\overline{DR},NLO}$	$\sigma^{\overline{DR},LO}$	$\sigma^{DCPR,NLO}$	$\sigma^{DCPR,LO}$	$K^{\overline{DR}}$	K^{DCPR}	NLO ratio
10	1.338	1.260	1.340	1.234	1.061	1.086	0.998
20	5.133	4.857	5.099	4.334	1.056	1.176	1.006
30	10.975	10.461	10.715	8.488	1.049	1.262	1.024
40	18.613	17.918	17.811	13.248	1.038	1.344	1.045

TABLE IV. h^0 production SPP_2 spectra: total cross sections (pb), K-factors, and NLO $\overline{DR}$/DCPR ratio.

$\tan\beta$	$\sigma^{\overline{DR},NLO}$	$\sigma^{\overline{DR},LO}$	$\sigma^{DCPR,NLO}$	$\sigma^{DCPR,LO}$	$K^{\overline{DR}}$	K^{DCPR}	NLO ratio
10	0.282	0.248	0.282	0.243	1.135	1.156	1.002
20	0.255	0.254	0.254	0.230	1.005	1.107	1.003
30	0.228	0.258	0.230	0.217	0.882	1.059	0.988
40	0.204	0.267	0.213	0.211	0.764	1.012	0.955

From inspection of the figures, one can draw the following main conclusions:

(1) The K-factors for H^0, A^0 are systematically small for large $\tan\beta$, and would reach a larger size (roughly, 8%) for small $\tan\beta$ values around 10.

(2) The K-factor for h^0 varies drastically with $\tan\beta$, changing from positive values of about 15% for $\tan\beta$ around 10 to negative values of about 25% for $\tan\beta$ around 40. These extreme negative and positive values are of a size that cannot be ignored in a dedicated experimental analysis.

These features follow from the two-Higgs doublet model structure and the $h^0 - H^0$ mixing where α is close to $\beta - \pi/2$ leading to a $\tan\beta$ enhancement in the h^0 case but to a $1/\tan\beta$ suppression in the H^0, A^0 cases.

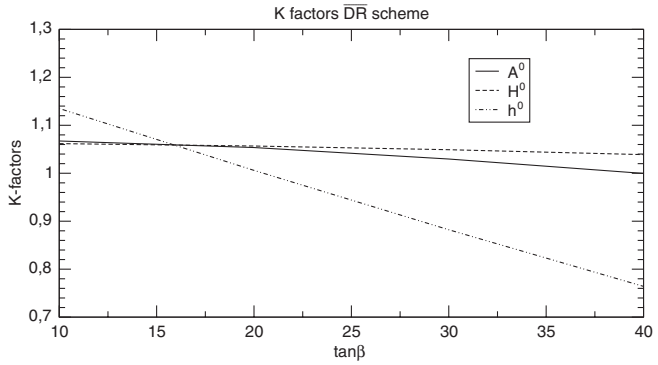

FIG. 11. K-factors for A^0, H^0, and h^0 production, $\overline{DR}$ scheme. $M_{A^0} = 250$ GeV, $p_{b,T} > 20$ GeV, $|y_b| < 2$.

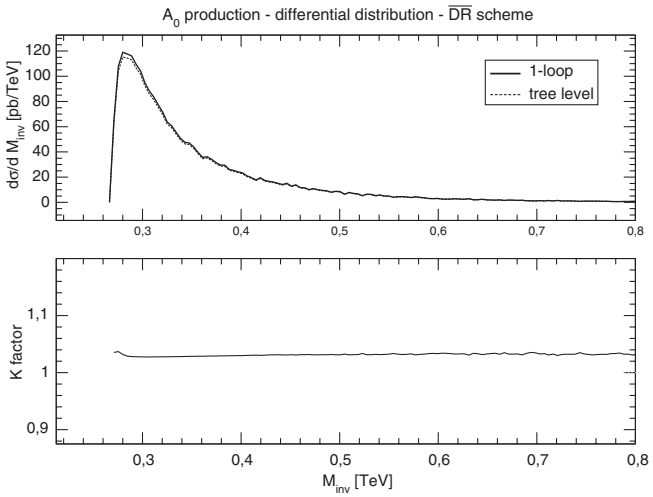

FIG. 12. Invariant mass distribution, A^0 production, $\overline{DR}$ scheme. $M_{A^0} = 250$ GeV, $\tan\beta = 30$, $p_{b,T} > 20$ GeV, $|y_b| < 2$.

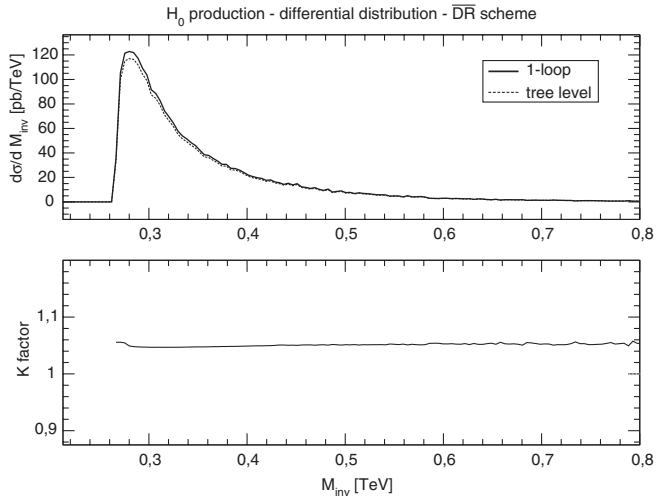

FIG. 13. Invariant mass distribution, H^0 production, $\overline{\mathrm{DR}}$ scheme. $M_{A^0} = 250$ GeV, $\tan\beta = 30$, $p_{b,T} > 20$ GeV, $|y_b| < 2$.

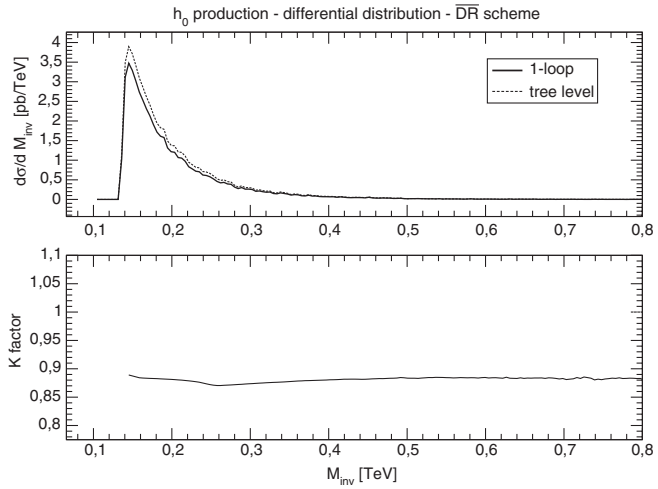

FIG. 14. Invariant mass distribution, h^0 production, $\overline{\mathrm{DR}}$ scheme. $M_{A^0} = 250$ GeV, $\tan\beta = 30$, $p_{b,T} > 20$ GeV, $|y_b| < 2$.

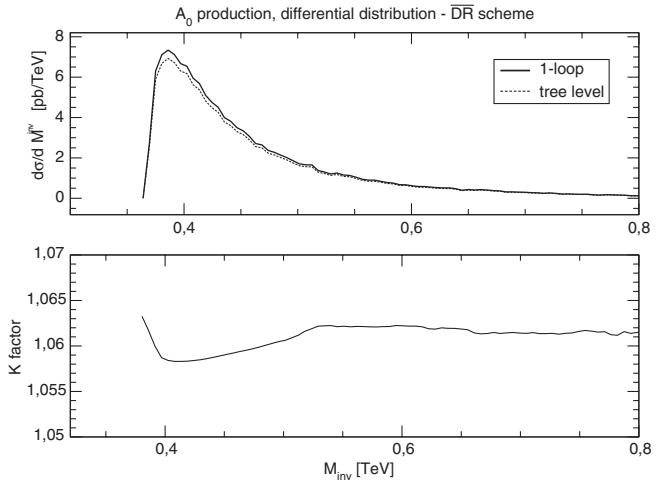

FIG. 15. Invariant mass distribution, A^0 production, $\overline{\mathrm{DR}}$ scheme. $M_{A^0} = 350$ GeV, $\tan\beta = 15$, $p_{b,T} > 20$ GeV, $|y_b| < 2$.

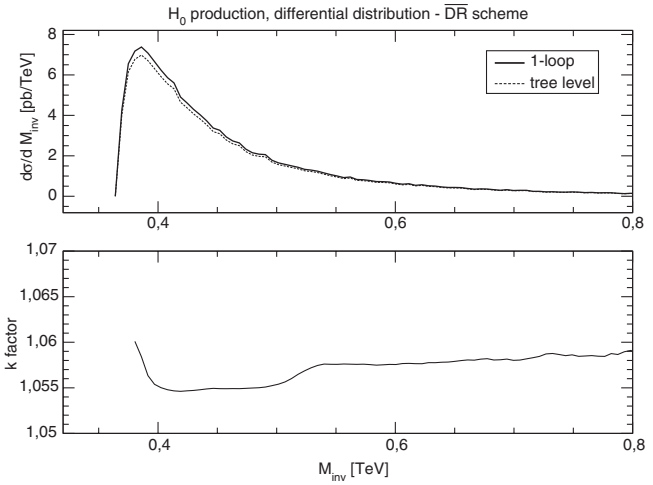

FIG. 16. Invariant mass distribution, H^0 production, $\overline{\mathrm{DR}}$ scheme. $M_{A^0} = 350$ GeV, $\tan\beta = 15$, $p_{b,T} > 20$ GeV, $|y_b| < 2$.

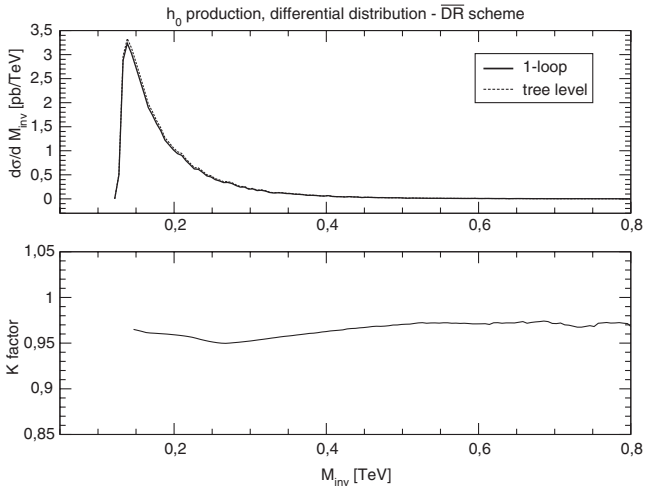

FIG. 17. Invariant mass distribution, h^0 production, $\overline{\mathrm{DR}}$ scheme. $M_{A^0} = 350$ GeV, $\tan\beta = 15$ $p_{b,T} > 20$ GeV, $|y_b| < 2$.

This, we believe, is the main message of our calculation: while for sure the QCD NLO are the dominant corrections (of order 20–40% depending on the Higgs mass; see for example [3]), as it was to be expected from the analysis of Dittmaier *et al.* [5], the one-loop electroweak contribution

TABLE V. SPP_1 spectrum: total cross sections (pb) for the three Higgs and $\overline{\mathrm{DR}}$ K-factors.

$\mathcal{H}^0$	$\sigma^{\overline{\mathrm{DR}},\mathrm{NLO}}$	$\sigma^{\overline{\mathrm{DR}},\mathrm{LO}}$	$K^{\overline{\mathrm{DR}}}$
A^0	0.768	0.724	1.060
H^0	0.769	0.727	1.056
h^0	0.213	0.222	0.961

in the semi-inclusive bottom-Higgs production processes must not be *a priori* considered as negligible.

IV. NUMERICAL APPROXIMATIONS

Having performed the calculation of complete one-loop effect on the process, we shall consider the possibility of simpler, effective approximations to the full and long calculation, that may be used to obtain a quicker and qualitative description of the results.

With this purpose we have first considered the ''improved Born approximation'' (IBA) following the prescriptions given in [5]: the IBA is obtained is this case by including in the definition of Δ_b [see Eq. (14)] the electroweak contributions and then replacing the mixing angle α with the effective value $\alpha_{\rm eff}$, obtained by the diagonalization of the one-loop mass matrix

$$\begin{pmatrix} m^2_{h^0} - \hat{\Sigma}_{h^0}(m^2_{h^0}) & -\hat{\Sigma}_{h^0H^0}\left(\frac{1}{2}(m^2_{h^0} + m^2_{H^0})\right) \\ -\hat{\Sigma}_{h^0H^0}\left(\frac{1}{2}(m^2_{h^0} + m^2_{H^0})\right) & m^2_{H^0} - \hat{\Sigma}_{H^0}(m^2_{H^0}) \end{pmatrix}. \tag{27}$$

The effect of the latter redefinition of α is negligible for H^0 and A^0, but significant for h^0.

As one can see from the plots (Figs. 18–20) this version of IBA is sufficiently close to the complete calculation only for relatively small $\tan\beta$ values, roughly $\tan\beta < 20$. In this range, the approximation gives larger (compared to the complete calculation) rates for H^0, A^0 and smaller rates for h^0. The differences remain below the 10% size, which would be tolerable at least in a first phase of LHC measurements. Increasing the $\tan\beta$ value, the IBA description becomes worse. For $\tan\beta = 40$, it differs in all the three cases by, roughly, a relative 25%, which seems a rather poor prediction for the measurable total rates.

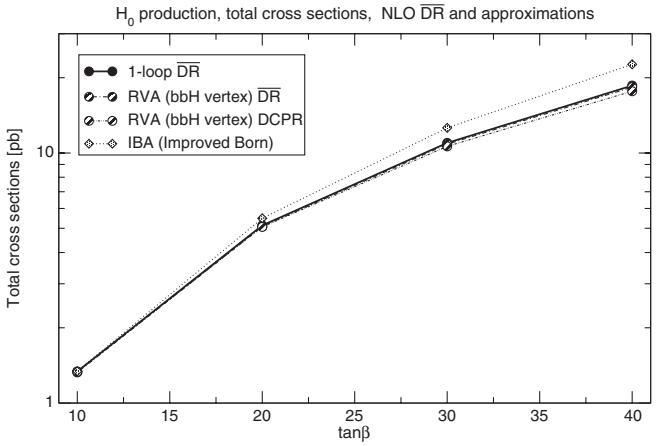

FIG. 19. Comparison of the total NLO cross sections: NLO $\overline{\rm DR}$, RVA ($\overline{\rm DR}$ and DCPR), and improved Born approximation, H^0 production; $M_{A^0} = 250$ GeV, $p_{b,T} > 20$ GeV, $|y_b| < 2$.

For what concerns the $\tan\beta$ dependence of the plots, one can conclude that it provides those features that would be expected at the chosen value of M_{A^0}, which is sufficiently larger than M_Z to approach the correct decoupling limits. In this large M_{A^0} regime, that is discussed widely in the literature (see e.g. [30]), the H^0 and A^0 couplings become almost exactly proportional to $\tan\beta$, while the h^0 coupling becomes very weakly $\tan\beta$ dependent. These features are well reproduced by the plots, that show a roughly quadratic $\tan\beta$ dependence of the H^0, A^0 rates and a much weaker $\tan\beta$ dependence for h^0. But for large $\tan\beta$ values, there seems to be an extra $\tan\beta$ dependence of the complete calculation that is not contained in the IBA description.

Having this apparent discrepancy in our mind, as a second attempt, we have tried to use what we would call a ''reduced vertex approximation'' (RVA): we approximate

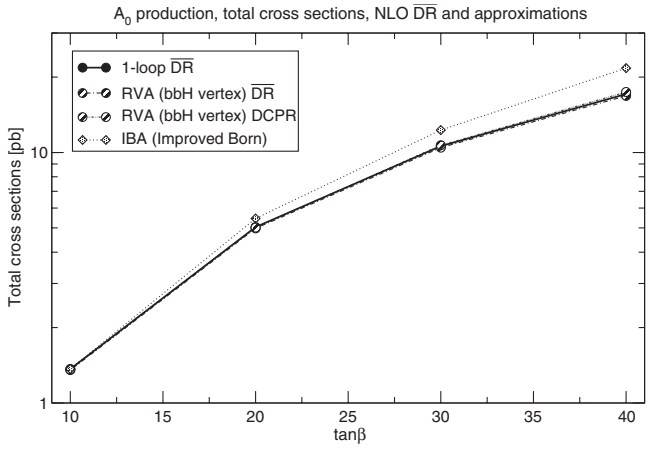

FIG. 18. Comparison of the total NLO cross sections: NLO $\overline{\rm DR}$, RVA ($\overline{\rm DR}$ and DCPR), and improved Born approximation, A^0 production; $M_{A^0} = 250$ GeV, $p_{b,T} > 20$ GeV, $|y_b| < 2$.

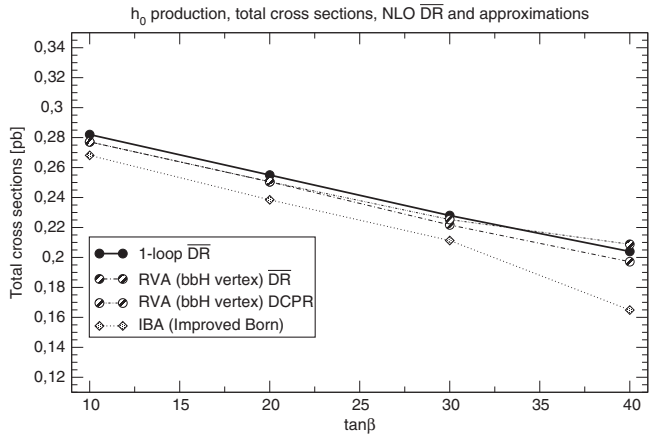

FIG. 20. Comparison of the total NLO cross sections: NLO $\overline{\rm DR}$, RVA ($\overline{\rm DR}$ and DCPR), and improved Born approximation, h^0 production; $M_{A^0} = 250$ GeV, $p_{b,T} > 20$ GeV, $|y_b| < 2$.

TABLE VI. H^0 production: comparison between the complete NLO prediction and the two approximations, total cross sections and ratios $\sigma^{\overline{\mathrm{DR}},\mathrm{NLO}}/\sigma_{\mathrm{APP.}}$.

$\tan\beta$	$\sigma^{\overline{\mathrm{DR}},\mathrm{NLO}}$	$\mathrm{RVA}_{bb\mathcal{H}}$	$\sigma/\mathrm{RVA}_{bb\mathcal{H}}$	IBA	σ/IBA
10	1.338	1.326 23	1.008 88	1.340 87	0.997 861
20	5.133	5.083 24	1.009 79	5.483 97	0.936
30	10.975	10.8433	1.012 15	12.6044	0.87073
40	18.613	18.3461	1.014 55	22.6229	0.822 749

TABLE VII. h^0 production: comparison between the complete NLO prediction and the two approximations, total cross sections and ratios $\sigma^{\overline{\mathrm{DR}},\mathrm{NLO}}/\sigma_{\mathrm{APP.}}$.

$\tan\beta$	$\sigma^{\overline{\mathrm{DR}},\mathrm{NLO}}$	$\mathrm{RVA}_{bb\mathcal{H}}$	$\sigma/\mathrm{RVA}_{bb\mathcal{H}}$	IBA	σ/IBA
10	0.282	0.277 157	1.017 47	0.268 161	1.051 61
20	0.255	0.250 495	1.017 99	0.238 459	1.069 36
30	0.228	0.221 673	1.028 54	0.211 275	1.079 16
40	0.204	0.197 159	1.0347	0.164 874	1.237 31

TABLE VIII. A^0 production: comparison between the complete NLO prediction and the two approximations, total cross sections and ratios $\sigma^{\overline{\mathrm{DR}},\mathrm{NLO}}/\sigma_{\mathrm{APP.}}$.

$\tan\beta$	$\sigma^{\overline{\mathrm{DR}},\mathrm{NLO}}$	$\mathrm{RVA}_{bb\mathcal{H}}$	$\sigma/RVA_{bb\mathcal{H}}$	IBA	σ/IBA
10	1.367	1.353 28	1.010 14	1.367 37	0.999 729
20	5.04	4.980 26	1.011 99	5.4543	0.924 042
30	10.601	10.4581	1.013 66	12.2948	0.862 232
40	17.118	16.8292	1.017 16	21.7326	0.787 663

the complete NLO keeping only the (all) one-loop corrections to the final Yukawa $bb\mathcal{H}^0$ vertex and the subset of counterterms needed to get a UV-finite result; the photon mass is regulated (arbitrarily) as $M_\gamma = M_Z$ (and thus we do not include soft and hard radiation). We kept the one-loop Higgs masses in the kinematics as well as the Z-factors in the definition of the cross section; all the other diagrams (boxes, initial, and up triangles, Self-Energies) are neglected. As a check we computed the cross section in this approximation in both schemes (the subset of diagrams, with the right choice of counterterms, should be scheme independent). As one can see from the updated figures our RVA turns out to provide a very efficient description of the total NLO cross sections; the difference between the NLO and the RVA is of order of 1%, 3.4% in the worst case. This is numerically summarized in Tables VI, VII, and VIII, and Figs. 18–20.

From the inspection of those tables and figures we would conclude that the extra vertices that the RVA contains seem to provide the extra $\tan\beta$ dependence not predicted by the IBA in a reasonably satisfactory way, i.e. at the level of few percent in the full $\tan\beta$ range. This RVA cannot be transformed into simple analytical expressions. It tells us that the relative effect of a large set of Feynman diagrams, those that were not included in the approximation, is small, at the level of a few percent, which might be considered negligible for the first phase of LHC measurements.

V. CONCLUSIONS

We have performed in this paper a complete MSSM calculation of the electroweak NLO effect in the processes of semi-inclusive bottom-Higgs production. Our analysis has been performed for two choices of the M_{A^0} input parameter and for variable values of the $\tan\beta$ parameter defined in the $\overline{\mathrm{DR}}$ renormalization scheme. Although a more extended analysis of the parameter space would be interesting, we have found certain results that appear to us to be general and worth publishing. The first conclusion is that two different renormalization schemes appear to be practically identical at SUSY NLO as one would *a priori* expect. Working in the $\overline{\mathrm{DR}}$ scheme, that seemed to us to be somehow preferable, we have found that the pure electroweak one-loop effect in the three considered production

processes is of a size that might be relevant and therefore that this contribution cannot be ignored for a proper experimental analysis of the reactions.

There could exist simpler calculations involving a smaller (but still large) number of diagrams, that would provide a valid numerical result. We have seen that one possible improved Born approximation does not reproduce the correct result in a satisfactory way. We have also seen that another reduced vertex approximation (which considers only the one-loop correction to the Yukawa $bb\mathcal{H}^0$ vertex) appears to better approximate the full NLO.

However, if a theoretical prediction of the total cross section is requested at the percent level, which might be the hopefully desirable final LHC goal, our conclusion is that the complete one-loop calculation of the electroweak part that we have performed in this paper should be considered, together with the available, large, QCD corrections, as the correct proposal to offer to the experimental community.

There remains a couple of relevant points still to be investigated. The first is that of combining this analysis with an analogous one to be performed for the process of associated top-charged Higgs production, for which our group has already provided a complete one-loop electroweak analysis [26]. The second one is that of trying to relate the $\overline{\mathrm{DR}}$ $\tan\beta$ parameter, which is not a measurable quantity, to a measurable $\tan\beta$ (which could be defined for instance by $A^0 \to \tau^+\tau^-$ decay as suggested in [29]). This would allow one to draw plots where also the horizontal axis represents a measurable quantity. These points are, in our opinion, quite relevant but beyond the purposes of our analysis; work is in progress on these issues.

ACKNOWLEDGMENTS

We want to thank A. Djouadi for several fruitful discussions. E. M. would like to thank Heidi Rzehak and Jianhui Zhang for valuable comments and suggestions. E. M. is supported by the European Research Council under Advanced Investigator Grant No. ERC-AdG-228301.

APPENDIX A: RENORMALIZATION CONSTANTS IN THE HIGGS SECTOR

The renormalization constants of the wave function of the Higgs bosons A^0, h^0, H^0 and of the Goldstone boson G^0 are given by

$$\begin{aligned}
\delta\bar{Z}_{H^0H^0} &= \cos^2\alpha\,\delta Z_{H1} + \sin^2\alpha\,\delta Z_{H2},\\
\delta\bar{Z}_{H^0h^0} &= \sin\alpha\cos\alpha(\delta Z_{H2} - \delta Z_{H1}),\\
\delta\bar{Z}_{h^0h^0} &= \sin^2\alpha\,\delta Z_{H1} + \cos^2\alpha\,\delta Z_{H2},\\
\delta\bar{Z}_{A^0A^0} &= \sin^2\beta\,\delta Z_{H1} + \cos^2\beta\,\delta Z_{H2},\\
\delta\bar{Z}_{G^0A^0} &= \cos\beta\sin\beta(\delta Z_{H2} - \delta Z_{H1}),\\
\delta\bar{Z}_{h^0A^0} &= \delta\bar{Z}_{H^0A^0} = \delta\bar{Z}_{h^0G^0} = \delta\bar{Z}_{H^0G^0} = 0.
\end{aligned} \tag{A1}$$

The renormalization constants for the $c^\eta(bbh^0)$ and for the $c^\eta(bbH^0)$ couplings are obtained differentiating the tree-level expressions in Eq. (5),

$$\begin{aligned}
\delta c^\eta(bbh^0) &= \left(\frac{\delta g}{g} + \frac{\delta m_b}{m_b} - \frac{\delta M_W^2}{2M_W^2} - \frac{\delta\cos\beta}{\cos\beta}\right)c^\eta(bbh^0),\\
\delta c^\eta(bbH^0) &= \left(\frac{\delta g}{g} + \frac{\delta m_b}{m_b} - \frac{\delta M_W^2}{2M_W^2} - \frac{\delta\cos\beta}{\cos\beta}\right)c^\eta(bbH^0).
\end{aligned} \tag{A2}$$

$\delta\cos\beta$, δM_W^2, and δg, read as follows:

$$\begin{aligned}
\delta\cos\beta &= -\sin^2\beta\frac{\delta\tan\beta}{\tan\beta},\\
\delta M_W^2 &= \mathrm{Re}\Sigma_W(M_W^2),\\
\frac{\delta g}{g} &= \frac{\Sigma_{\gamma Z}(0)}{s_W c_W M_Z^2} - \frac{1}{2}\Bigg[+2\frac{c_W}{s_W M_Z^2}\Sigma_{\gamma Z}(0)\\
&\quad + \frac{c_W^2}{s_W^2}\left(\frac{\delta M_Z^2}{M_Z^2} - \frac{\delta M_W^2}{M_W^2}\right) - \Sigma'_{\gamma\gamma}(0)\Bigg],
\end{aligned} \tag{A3}$$

with $\delta M_Z^2 = \mathrm{Re}\Sigma_Z(M_Z^2)$. The $c^\eta(bbA^0)$ couplings depends only on the angle β. When computing the renormalization constant $\delta c^\eta(bbA^0)$, one has to distinguish between the β-dependent factors originated by the H_1, H_2 mixing and the β-dependent factors from the H_1, H_2 couplings. Only the latter have to be renormalized. In particular the factor $\sin\beta$ $(1/\cos\beta)$ entering the $c^\eta(bbA^0)$ coupling is originated from the H_1, H_2 mixing (couplings), and thus $\delta c^\eta(bbA^0)$ reads

$$\delta c^\eta(bbA^0) = \left(\frac{\delta g}{g} + \frac{\delta m_b}{m_b} - \frac{\delta M_W^2}{2M_W^2} - \frac{\delta\cos\beta}{\cos\beta}\right)c^\eta(bbA^0). \tag{A4}$$

APPENDIX B: CONTRIBUTIONS OF THE COUNTERTERMS

In this appendix we list explicitly the contributions of the counterterms written in terms of the renormalization constants introduced in Sec. II C and in Appendix A. The vertices' counterterms can be written as follows:

$$\bar{u}'_b(\lambda'_b)\left(\sum_{k=1}^{4}\sum_{\eta=L,R} J^{k\eta} V^{k\eta}_{bg\to b\mathcal{H}^0}\right)u_b(\lambda_b), \tag{B1}$$

where $J^{k\eta}$ are defined in Eq. (8) while the nonzero $V^{k\eta}_{bg\to b\mathcal{H}^0}$ reads

$$
\begin{aligned}
V^{1\eta}_{bg\to b\mathcal{H}^0} &= \frac{g_s}{s-m_b^2}\left\{\left(\frac{3}{2}\delta Z^b_\eta+\frac{1}{2}\delta Z^b_{\bar\eta}\right)c^\eta(bb\mathcal{H}^0)+\delta c^\eta(bb\mathcal{H}^0)+\frac{1}{2}\sum_{\bar{\mathcal{H}}^0}\delta\bar Z^*_{\bar{\mathcal{H}}^0\mathcal{H}^0}c^\eta(bb\bar{\mathcal{H}}^0)\right\}\\
&\quad-\frac{g_s}{u-m_b^2}\left\{\left(\frac{3}{2}\delta Z^b_{\bar\eta}+\frac{1}{2}\delta Z^b_\eta\right)c^\eta(bb\mathcal{H}^0)+\delta c^\eta(bb\mathcal{H}^0)+\frac{1}{2}\sum_{\bar{\mathcal{H}}^0}\delta\bar Z^*_{\bar{\mathcal{H}}^0\mathcal{H}^0}c^\eta(bb\bar{\mathcal{H}}^0)\right\},\\
V^{2\eta}_{bg\to b\mathcal{H}^0} &= \frac{-2g_s}{u-m_b^2}\left\{\left(\frac{3}{2}\delta Z^b_{\bar\eta}+\frac{1}{2}\delta Z^b_\eta\right)c^\eta(bb\mathcal{H}^0)+\delta c^\eta(bb\mathcal{H}^0)+\frac{1}{2}\sum_{\bar{\mathcal{H}}^0}\delta\bar Z^*_{\bar{\mathcal{H}}^0\mathcal{H}^0}c^\eta(bb\bar{\mathcal{H}}^0)\right\},\\
V^{3\eta}_{bg\to b\mathcal{H}^0} &= \frac{m_b g_s}{s-m_b^2}(\delta Z^b_{\bar\eta}-\delta Z^b_\eta)c^{\bar\eta}(bb\mathcal{H}^0)+\frac{m_b g_s}{u-m_b^2}(\delta Z^b_{\bar\eta}-\delta Z^b_\eta)c^\eta(bb\mathcal{H}^0),
\end{aligned}
\tag{B2}
$$

where $(\eta,\bar\eta)\in\{(L,R);(R,L)\}$ and $\mathcal{H}^0$, $\bar{\mathcal{H}}^0=h^0,H^0,A^0,G^0$. The bottom self-energy counterterm reads as follows

$$
\bar u'_b(\lambda'_b)\left(\sum_{k=1}^{4}\sum_{\eta=L,R}J^{k\eta}S^{k\eta}_{bg\to b\mathcal{H}^0}\right)u_b(\lambda_b).
\tag{B3}
$$

The nonzero $S^{k\eta}_{bg\to b\mathcal{H}^0}$ are

$$
\begin{aligned}
S^{1\eta}_{bg\to b\mathcal{H}^0} &= g_s\frac{c^\eta(bb\mathcal{H}^0)}{(s-m_b^2)^2}\left\{s\delta Z^b_\eta-m_b^2\left(\delta Z^b_\eta-2\frac{\delta m_b}{m_b}\right)\right\}+g_s\frac{c^\eta(bb\mathcal{H}^0)}{(u-m_b^2)^2}\left\{u\delta Z^b_{\bar\eta}-m_b^2\left(\delta Z^b_{\bar\eta}-2\frac{\delta m_b}{m_b}\right)\right\}\\
S^{2\eta}_{bg\to b\mathcal{H}^0} &= 2g_s\frac{c^\eta(bb\mathcal{H}^0)}{(u-m_b^2)^2}\left\{u\delta Z^b_{\bar\eta}-m_b^2\left(\delta Z^b_{\bar\eta}-2\frac{\delta m_b}{m_b}\right)\right\}\\
S^{3\eta}_{bg\to b\mathcal{H}^0} &= g_s m_b\frac{c^{\bar\eta}(bb\mathcal{H}^0)}{(s-m_b^2)}\left\{\frac{1}{2}(\delta Z^b_\eta-\delta Z^b_{\bar\eta})-\frac{\delta m_b}{m_b}\right\}+g_s m_b\frac{c^\eta(bb\mathcal{H}^0)}{(u-m_b^2)}\left\{\frac{1}{2}(\delta Z^b_\eta-\delta Z^b_{\bar\eta})-\frac{\delta m_b}{m_b}\right\}.
\end{aligned}
\tag{B4}
$$

[1] J. M. Campbell *et al.*, in *Higgs Boson Production in Association with Bottom Quarks*, Proceedings of the Les Houches Summer School, Session III (World Scientific, Singapore, 2004).
[2] D. Dicus, T. Stelzer, Z. Sullivan, and S. Willenbrock, Phys. Rev. D **59**, 094016 (1999).
[3] J. M. Campbell, R. K. Ellis, F. Maltoni, and S. Willenbrock, Phys. Rev. D **67**, 095002 (2003).
[4] R. V. Harlander and W. B. Kilgore, Phys. Rev. D **68**, 013001 (2003).
[5] S. Dittmaier, M. Kramer, A. Muck, and T. Schluter, J. High Energy Phys. 03 (2007) 114.
[6] S. Dawson, C. B. Jackson, L. Reina, and D. Wackeroth, Phys. Rev. Lett. **94**, 031802 (2005).
[7] S. Dawson and C. B. Jackson, Phys. Rev. D **77**, 015019 (2008).
[8] S. Dawson and P. Jaiswal, Phys. Rev. D **81**, 073008 (2010).
[9] S. Dawson, C. B. Jackson, L. Reina, and D. Wackeroth, Mod. Phys. Lett. A **21**, 89 (2006).
[10] Stefan Dittmaier, Michael Kramer, and Michael Spira, Phys. Rev. D **70**, 074010 (2004).
[11] S. Dawson, C. B. Jackson, L. Reina, and D. Wackeroth, Phys. Rev. D **69**, 074027 (2004).
[12] F. Boudjema and L. D. Ninh, Phys. Rev. D **77**, 033003 (2008).
[13] G. Gao, R. J. Oakes, and J. M. Yang, Phys. Rev. D **71**, 095005 (2005).
[14] M. Frank, T. Hahn, S. Heinemeyer, W. Hollik, H. Rzehak, and G. Weiglein, J. High Energy Phys. 02 (2007) 047.
[15] A. Dabelstein, Z. Phys. C **67**, 495 (1995).
[16] P. H. Chankowski, S. Pokorski, and J. Rosiek, Nucl. Phys. **B423**, 437 (1994).
[17] S. Heinemeyer, W. Hollik, H. Rzehak, and G. Weiglein, Eur. Phys. J. C **39**, 465 (2005).
[18] J. Kublbeck, M. Bohm, and A. Denner, Comput. Phys. Commun. **60**, 165 (1990); T. Hahn, Comput. Phys. Commun. **140**, 418 (2001); T. Hahn and C. Schappacher, Comput. Phys. Commun. **143**, 54 (2002);
[19] T. Hahn and M. Perez-Victoria, Comput. Phys. Commun. **118**, 153 (1999).T. Hahn and M. Rauch, Nucl. Phys. B, Proc. Suppl. **157**, 236 (2006).
[20] V. N. Baier, V. S. Fadin, and V. A. Khoze, Nucl. Phys. **B65**, 381 (1973).
[21] U. Baur, S. Keller, and D. Wackeroth, Phys. Rev. D **59**, 013002 (1998).
[22] S. Dittmaier, Nucl. Phys. **B565**, 69 (2000).

[23] S. Heinemeyer, W. Hollik, and G. Weiglein, Comput. Phys. Commun. **124**, 76 (2000).
[24] J. H. Kuhn, A. Kulesza, S. Pozzorini, and M. Schulze, Nucl. Phys. **B797**, 27 (2008).
[25] M. Beccaria, G. Macorini, E. Mirabella, L. Panizzi, F. M. Renard, and C. Verzegnassi, Int. J. Mod. Phys. A **24**, 5539 (2009).
[26] M. Beccaria, G. Macorini, L. Panizzi, F. M. Renard, and C. Verzegnassi, Phys. Rev. D **80**, 053011 (2009).
[27] J. Pumplin, D. R. Stump, J. Huston, H. L. Lai, P. M. Nadolsky, and W. K. Tung, J. High Energy Phys. 07 (2002) 012.
[28] M. Roth and S. Weinzierl, Phys. Lett. B **590**, 190 (2004).
[29] See A. Freitas and D. Stockinger, Phys. Rev. D **66**, 095014 (2002), and references therein.
[30] A. Djouadi, Phys. Rep. **459**, 1 (2008).